Abstract

Keywords:

1. Introduction

The search for alternate energy sources which could be categorised under the "green" label has become important area of research in the modern word. Solar, wind power and wave power are some of the examples of these sources. Recently,a new branch of research has been developing to extract energy from flow induced vibrations(Bernitsas et al. (2008)). It has been hypothesized that this technique may work efficiently in areas where regular turbines cannot.

A simple structure that is susceptible to flow-induced vibrations that are suitable for energy extraction are slender structures,such as cylinders, elastically mounted perpendicular to a fluid stream. With regards to a slender body two common types of flow induced vibrations are Vortex Induced Vibrations (VIV) and aeroelastic galloping. Significant research has been carried out by Bernitsas and his team on extracting useful energy from VIV. Some of their significant work includes investigating the influence of physical parameters such as mass ratio (the ratio of the mass of the cylinder and the displaced fluid), Reynolds number, mechanical properties(Raghavan and Bernitsas (2011) ,Lee and Bernitsas (2011)) and location (effect of the bottom boundary) (Raghavan et al. (2009)). However,the possibility of extracting energy using aeroelastic galloping has not been thoroughly investigated. Some theoretical work was carried out by (Barrero-Gil et al. (2010)). Utilizing galloping may be a more viable method to harness energy from flow induced vibrations as it is not bounded by a "lock-in" range of reduced velocities(ratio between the freestream velocity and the product of the natural frequency of the system and the characteristic length).Therefore it is preferable to investigate further the possibility of harnessing energy from flow induced vibrations using aeroelastic galloping.

Real life energy harvesting systems use high damping ratios where the energy generator (e.g electrical generator) puts a significant amount of damping into the system. Therefore it is crucial to investigate the behaviour of aeroleastic galloping scenarios at high damping ratios in order to optimise the system to obtain a acceptable power output.Hence the focus of this paper is concentrated on investigating the mechanical power output of high-damped galloping systems in laminar flow.

According to Païdoussis et al. (2010),Glauert (1919) has provided a criterion for galloping by considering the auto-rotation of an aerofoil. Den Hartog (1956) has provided a theoretical explanation for galloping for iced electric transmission lines. A non-linear theoretical aeroelastic model to predict the response of galloping was developed by Parkinson and Smith (1964) based on the quasi-steady state (QSS) theory. Experimental lift and drag data on a fixed square prism at different angles of attack were used as an input

for the theoretical model. It essentially used a curve fit of the transverse force to predict the galloping response. The study managed to achieve a good agreement with experimental (wind tunnel) data.Joly et al. (2012) have observed that finite element simulations shows a sudden change in amplitudes below a critical values of the mass ratio, which the (QSS) model fails to reproduce.The Parkinson's equation was essentially modified to account for the vortex shedding and managed to produce the effects to the amplitude at low mass ratios. Barrero-Gil et al. (2010) have investigated the possibility of extracting power from vibrations caused by galloping using quasi-steady state theory. In the conclusions of that paper it was pointed out that in order to obtain a high power to area ratio the mass-damping ($m^*\zeta$) parameter should be kept low as well as the frequency of oscillations should be carefully matched have a good agreement with the size of the cross section. Another interesting conclusion was that energy conversion systems which uses galloping could operate over a large range of flow velocities unlike VIV energy harvesting systems where the factor of energy conversion has a strong dependence on the incoming flow velocity.

Nomenclature

a_1, a_3, a_5, a_7	coefficients of the polynomial to determine C_y
F_y	force due to C_y
ρ	fluid density
m	mass of the body
m_a	added mass
c	damping constant/damping factor
k	spring constant
U	freestram velocity
$y, \dot{y}, \ddot{y}$	transverse displacement,velocity and acceleration
A	displacement amplitude
F_0	force due to shedding
ω_s	vortex shedding frequency
t	time
P_{mean}	mean power
$f = \frac{1}{2\pi}\sqrt{\frac{k}{m}}$	natural frequency of the system
$\omega_n = 2\pi f$	natural frequency of the system
D	characteristic length of the body
$m^* = \frac{m}{\rho \times \text{Volume of the body}}$	mass ratio
$U^* = \frac{U}{f \times D}$	reduced velocity
$\zeta = \frac{c}{2m\omega_n}$	damping ratio
P_t	power transferred to the body by the fluid
P_d	power dissipated due to mechanical damping
$\theta = \tan^{-1}\left(\frac{\dot{y}}{U}\right)$	instantaneous angle

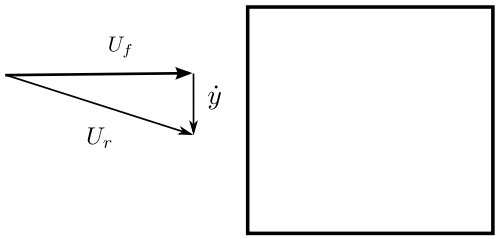

Figure 1

2. Background theory

2.1. Mathematical model (Quasi-steady)

One of the widely used mathematical model to predict the system response under galloping is the Quasi-steady state (QSS) model, incorporated by Parkinson and Smith (1964) for a square cross section. The equation of motion of the body under galloping is given by Eq. (1). The forcing term F_y is given by Eq.(2).

$$(m + m_a)\ddot{y} + c\dot{y} + ky = F_y \tag{1}$$

$$F_y = \frac{1}{2}\rho U^2 C_y \tag{2}$$

In the QSS model C_y is determined by an interpolating polynomial based on the stationary lift and drag data. The order of the interpolation polynomial has varied from study to study (e.g..7^{th} order was used in Parkinson and Smith (1964) and 3^{rd} order polynomial was used in Barrero-Gil et al. (2009). Ng et al. (2005) concluded that using a 7^{th} order polynomial is sufficient and a polynomial higher than that of 7^{th} order polynomial neither results in a result significantly better result nor does it exhibit an additional amplitudes of oscillation. Thus A 7^{th} order interpolating polynomial is incorporated in this present study.

$$C_y(\alpha) = a_1\left(\frac{\dot{y}}{U}\right) + a_3\left(\frac{\dot{y}}{U}\right)^3 + a_5\left(\frac{\dot{y}}{U}\right)^5 + a_7\left(\frac{\dot{y}}{U}\right)^7 \tag{3}$$

Joly et al. (2012) used a sinusoidal forcing function to the RHS of the oscillator model (Eq. (1)) in order to represent forcing due to VIV. This method provided satisfactory results with the numerical simulations obtained at low mass ratios. This study, the forcing due to VIV is incorporated using a sinusoidal forcing function $F_0 \sin \omega_s t$ added to the RHS. ω_s and F_0 represents shedding frequency and the maximum force due to shedding respectively. Thus, the final equation is represented by Eq. (4).

$$(m+m_a)\ddot{y}+c+\dot{y}+ky=\frac{1}{2}\rho U^2 \mathrm{A}\left(a_1\left(\frac{\dot{y}}{U}\right)+a_3\left(\frac{\dot{y}}{U}\right)^3+a_5\left(\frac{\dot{y}}{U}\right)^5+a_7\left(\frac{\dot{y}}{U}\right)^7\right)+F_0\sin(\omega_s t) \tag{4}$$

This equation could be solved by time integration methods. In this study "Ode 45" routine in MATLAB was used to obtain the solutions.

2.2. Calculation of average power

The dissipated power due to the damper could be expressed as the harvested power output assuming that the other power dissipation due to internal damping such as friction of the system is negligible. Therefore the mean power output could be given by Eq. (5).

$$P_{mean} = \frac{1}{T}\int_0^T (c\dot{y})\dot{y}dt \tag{5}$$

2.3. Parameters used

The stationary data and the FSI data were obtained using a higher order spectral element code which simulates 2D laminar flow. The Reynolds number was kept at 165 as it was pointed out by Sheard et al. (2009) and Tong et al. (2008) that the 3 dimensional transition for a square cylinder occurs at approximately Re-160. F_0 was kept at 0.4937 which was obtained by using a simple linear interpolation on the data of Joly et al. (2012). ω_s was set to 0.98 winch was obtained by a power spectral analysis of the stationary data at 0^0. Stationary C_y data were obtained at different angles of attack ranging from 0^0 to 16^0. The average power was obtained by using Eq. (5) with data sets consisting substantial amount of peaks. In order to obtain a comparison with high Reynolds number power data was obtained using Parkinson and Smith (1964) C_y data.

FSI data were obtained for the oscillating (free-vibration) scenario. The Naiver-Stokes equations were solved using an accelerated frame of reference using the previously mentioned code. A three-step time splitting scheme together with high-order Lagrangian polynomials were used to obtain the solution. The details of the method could be found in Thompson et al. (2006, 1996). This code was incorporated in Leontini et al. (2011, 2007) where it was employed in a fluid-structure interaction problems.

The computational domain consists of 690 quadrilateral macro elements(refer figure) where majority of the elements were concentrated near the square section. A freestream condition was given to the inlet, top and bottom boundaries and the normal velocity gradient was set to zero at the outlet. A convergence study was performed by changing the order of the polynomial (p-refinement) at $U^* = 40$ and Re 165. A 9th order polynomial together with a time step of $\frac{\Delta tU}{D} = 0.001$ was sufficient to ensure an accuracy of 2% with regards to amplitude of oscillation.

3. Results

3.1. Displacement,velocity and power output as a function of reduced velocity

The quasi-steady analysis data reveals that the displacement amplitude tend to grow with increasing U^* Fig.3. The onset of galloping is delayed with increasing ζ.

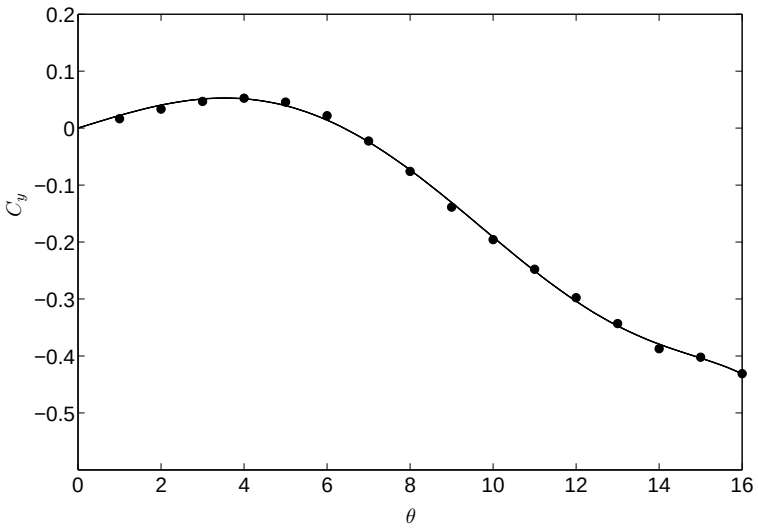

Figure 2

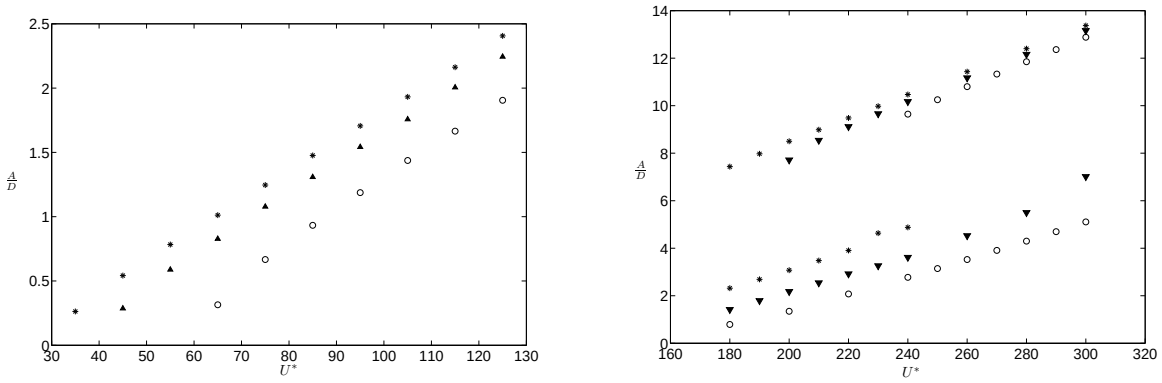

(a) $*$ $\zeta = 0.075$ ▲ $\zeta = 0.15$ $*$ $\zeta = 0.15$ (b) $*$ $\zeta = 0.0125$ ▼ $\zeta = 0.015$ $*$ $\zeta = 0.0175$

Figure 3: Displacement amplitude vs U^* at different ζ (a) Re 165 (b) Parkinson data

Power vs U^*

The mean power grows, peaks and then reduces as U^* is increased Fig.5. A shift of the peak power could be observed as ζ increases. However, the magnitude of the peaks remain constant for all the values of ζ. A similar observation could be made from the results of Barrero-Gil et al. (2010). It could be observed that unlike VIV the system has no preferred frequency. The onset of galloping and the peak power occurs at different U^* at when the damping ratio is changed. The peak power remains constant regardless of U^*.

3.2. Galloping response and natural frequency

If the oscillator equation Eq.(4) is considered from a power perspective (disregarding the shedding term as the net effect is zero), it could be seen that the forcing term on RHS

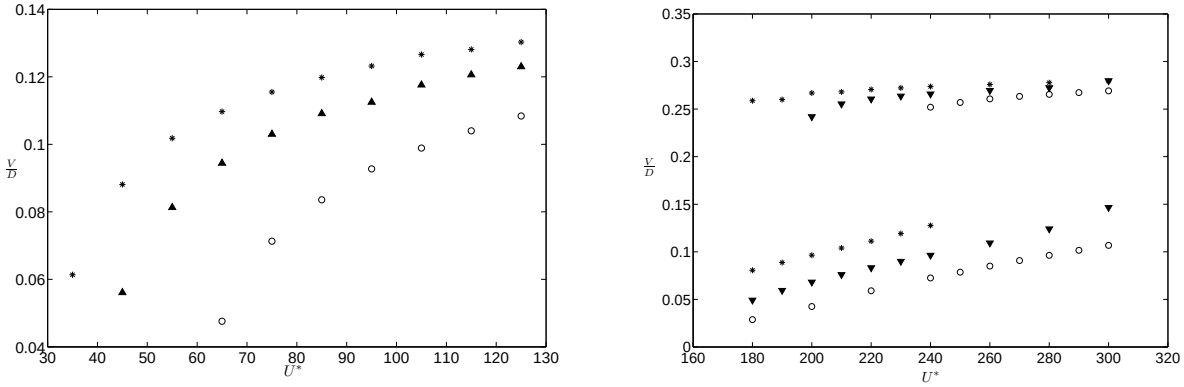

(a) $*\ \zeta = 0.075$ ▲ $\zeta = 0.15$ $*\ \zeta = 0.15$ (b) $*\ \zeta = 0.0125$ ▼ $\zeta = 0.015$ $*\ \zeta = 0.0175$

Figure 4: Velocity amplitude vs U^* at different ζ (a) Re 165 (b) Parkinson data

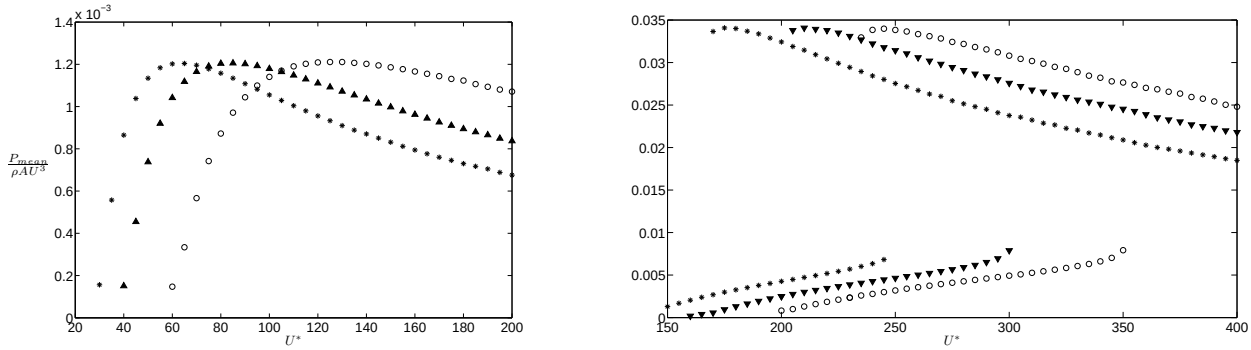

(a) $*\ \zeta = 0.075$ ▲ $\zeta = 0.15$ $*\ \zeta = 0.15$ (b) $*\ \zeta = 0.0125$ ▼ $\zeta = 0.015$ $*\ \zeta = 0.0175$

Figure 5: Mean power vs U^* at different ζ (a) Re 165 (b) Parkinson data

of the equation is only dependent on transverse velocity($\dot{y}$) which is essentially the input power of the system. On the RHS, the mechanical damping or system damping is the only term that takes out power at any instant by the product of damping force and the velocity (P_d). The inertia and the stiffness terms governs the frequency of the system the forces associated by those terms are conservative forces i.e there is zero net energy in or out of the system when averaged over a period. Therefore it appears that the system is governed by the transverse velocity rather than the natural frequency.

Using U^* and ζ assumes that the system has a preferred frequency. The effect of fixing ζ and increasing U^* actually decreases damping constant for a fixed free-stream velocity.($U^* = \frac{U}{f \times D}$, $\zeta = \frac{c}{2m\omega_n}$). Both these effects leads to the multiple lines that horizontally transpose when ζ is increased(Fig.5). Therefore the effect of ζ essentially scales up the damping coefficient for a fixed U.

Therefore a single set of results for a given a_1, a_3, a_5 and a_7 could be obtained if we were to plot displacement, velocity and power as a function of damping constant c (Fig 6,

7). A similar maximum velocity could be obtained for a given 'c'. Fig.8 clearly shows the validity of this argument.

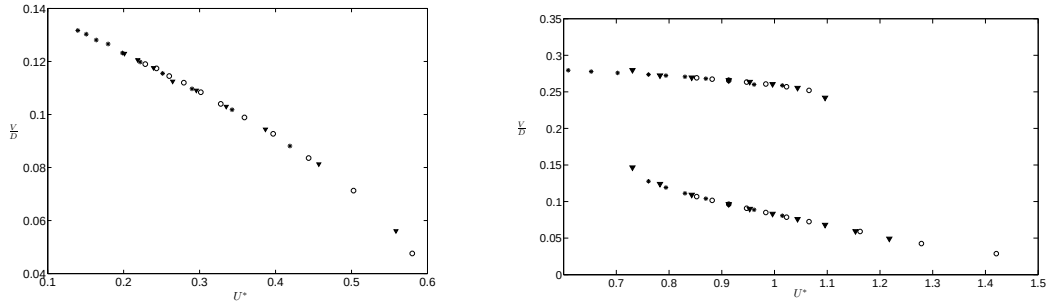

(a) $*\ \zeta = 0.075$ ▲ $\zeta = 0.15$ $*\ \zeta = 0.15$ (b) $*\ \zeta = 0.0125$ ▼ $\zeta = 0.015$ $*\ \zeta = 0.0175$

Figure 6: Velocity amplitude vs damping constant (a) Re 165 (b) Parkinson data

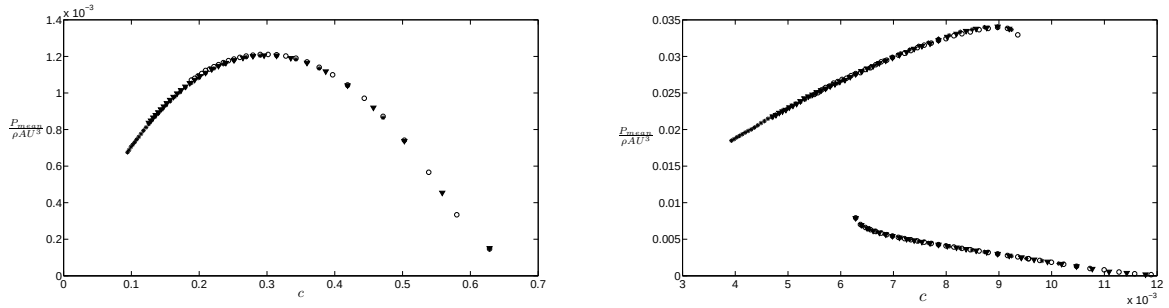

(a) $*\ \zeta = 0.075$ ▲ $\zeta = 0.15$ $*\ \zeta = 0.15$ (b) $*\ \zeta = 0.0125$ ▼ $\zeta = 0.015$ $*\ \zeta = 0.0175$

Figure 7: Mean power vs damping constant (a) Re 165 (b) Parkinson data

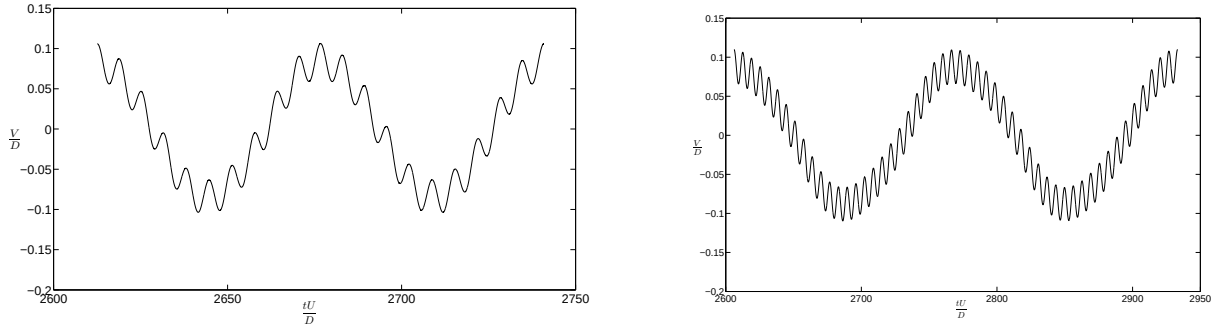

(a) (b)

Figure 8: Time history of velocity (a) $U^* = 60$ $\zeta = 0.075$ (b) $U^* = 150$ $\zeta = 0.0175$ at Re 165

Power could be expressed as the product of force and velocity. Therefore the transferred

power form fluid-to-body could be expressed as $P_t = F_y\dot{y}$. Similarly the dissipated power due to the mechanical damping could be expressed as $P_d = (c\dot{y})\dot{y}$.

The analysis of time histories of P_t and P_d at key regions (Fig.9) on the mean power vs U^* provides an detailed explanation on what exactly happens to power when the reduced velocity is increased. It has been established earlier that the damping factor is a function of U^*. It could be derived that U^* is inversely proportional to damping coefficient.

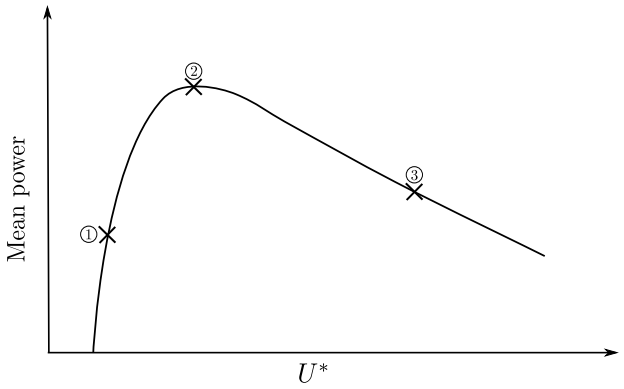

Figure 9: Three main regions of analysis of the Mean power Vs U^* curve

At region 3 ($U^* = 400$) 'c' is significantly low therefore the mean power output is less. From Fig. 10 it could be observed that P_t becomes negative. This is due to the fact that θ moves to a region where F_y becomes negative while velocity is positive. Hence P_t becomes positive. On the other hand in terms of an energy point of view, the mechanical damping is not sufficient to dissipate out the total transferred energy (as 'c' is substantially low), therefore part of it is transferred back to the fluid. At region 2 where the mean power becomes maximum($U = 165$), P_t does not become a pure sinusoidal signal. However, the signal remains periodic. From the time history graph of P_t two 'peaks' are present in a single half cycle (Fig 12). From Fig. 13 and 2 it could be observed that θ passes critical angle where the maximum C_y is produced. Therefore, the force F_y and P_t reduces as the velocity increases. As the velocity $\dot{y}$ is sinusoidal θ recovers back and leading to two 'peaks' in a single half cycle. $U^* = 90$ (region 1) the damping constant is high and therefore a clear sinusoidal signal could be observed for both P_d and P_t Fig. 14. From Fig. 2 and 15 it is possible to see that the θ does not exceed the critical angle where the maximum C_y (and therefore maximum F_y) is produced. Hence both P_d and P_t becomes sinusoidal.

3.3. Effect of m^*

The maximum mean power at different m^* Fig.16 was constant beyond $m^* = 30$. However, at $m^* \leq 30$ an effect of m^* could be observed, where the maximum of the mean power curve reduced as m^* was reduced. This may be due to the fact that shedding dominates as the inertia of the system is reduced. This was also reported by Joly et al. (2012) where an influence of vortex shedding was present on galloping amplitude at low mass ratios.

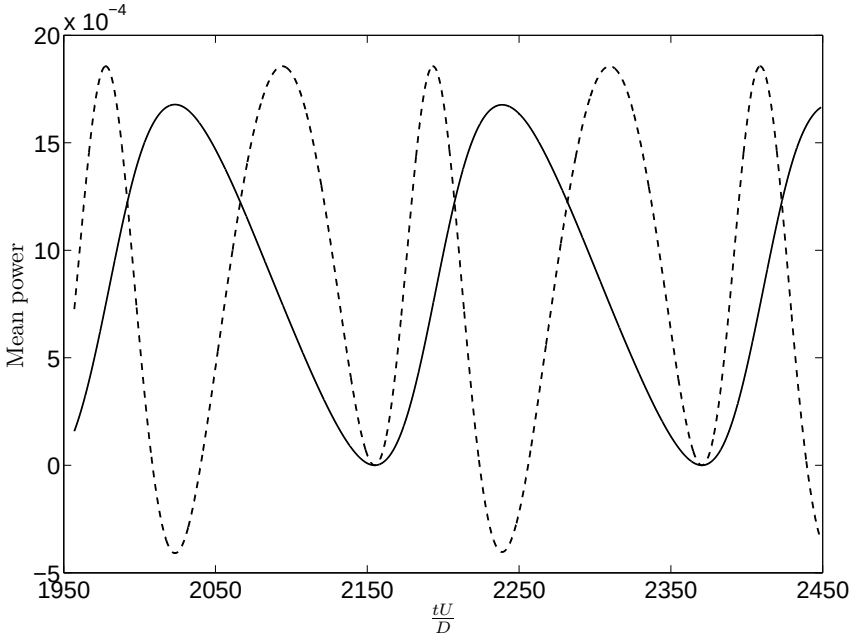

Figure 10: Time history of P_t - - - and P_d — at $U^* = 400$, $m^* = 40$ and $\zeta = 0.1$

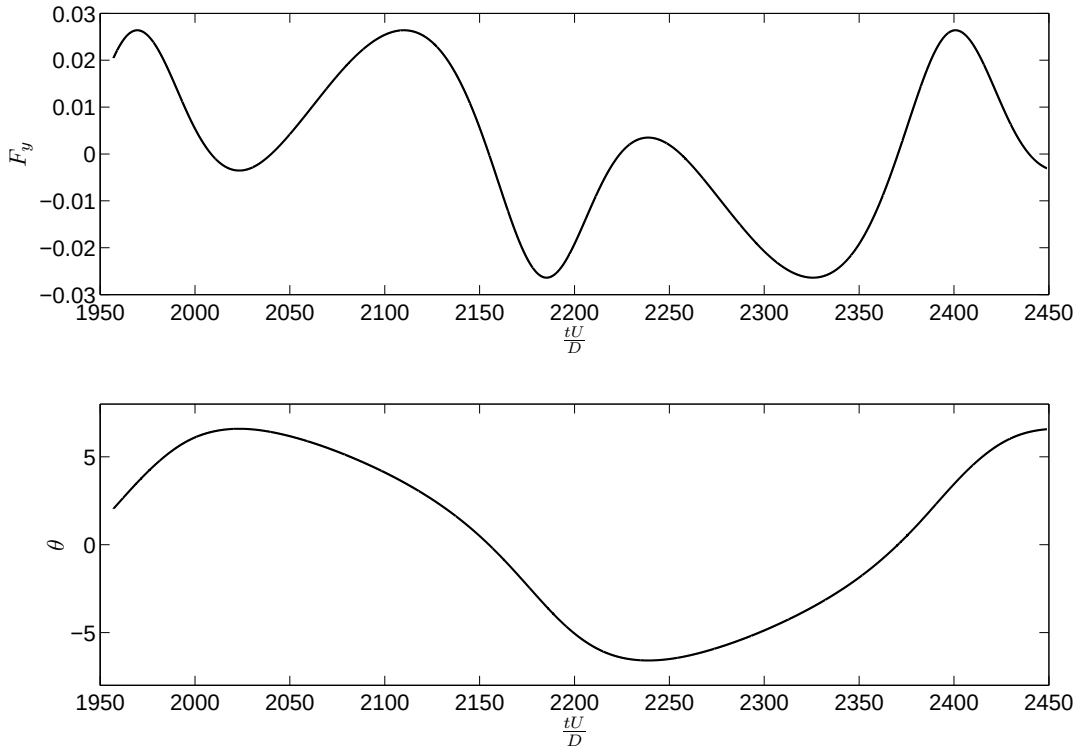

Figure 11: Time histories of θ and F_y at $U^* = 400$, $m^* = 40$ and $\zeta = 0.1$

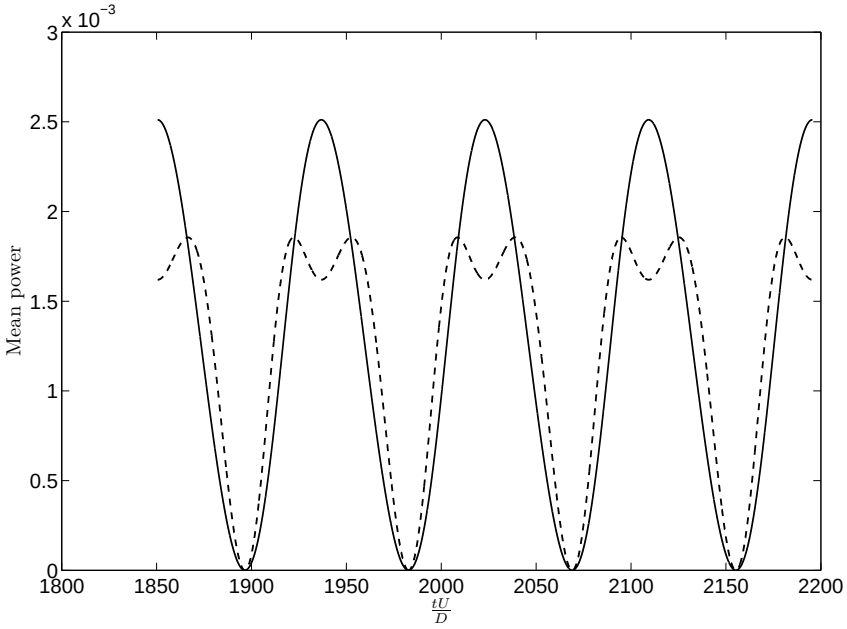

Figure 12: Time history of P_t - - - and P_d — at $U^* = 165$, $m^* = 40$ and $\zeta = 0.1$

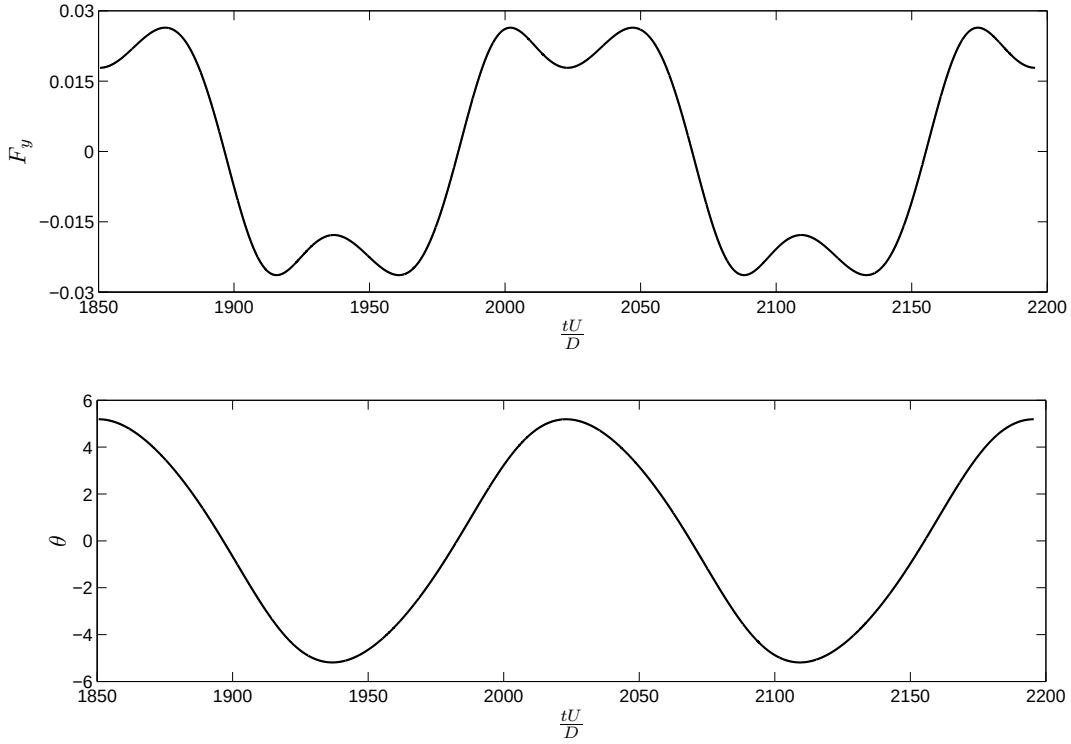

Figure 13: Time history of θ and f_y at $U^* = 400$, $m^* = 40$ and $\zeta = 0.1$

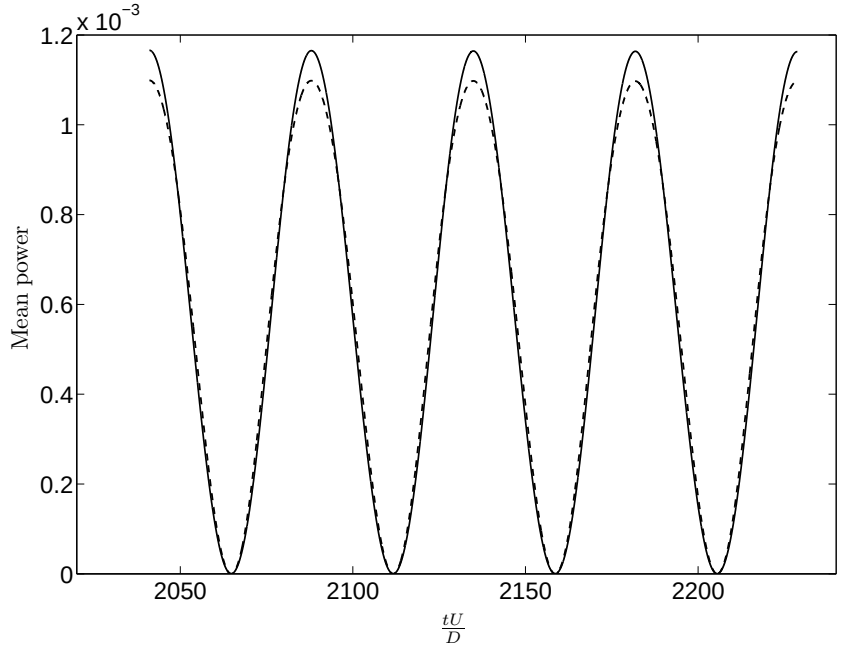

Figure 14: Time history of P_t - - - and P_d — at $U^* = 90$, $m^* = 40$ and $\zeta = 0.1$

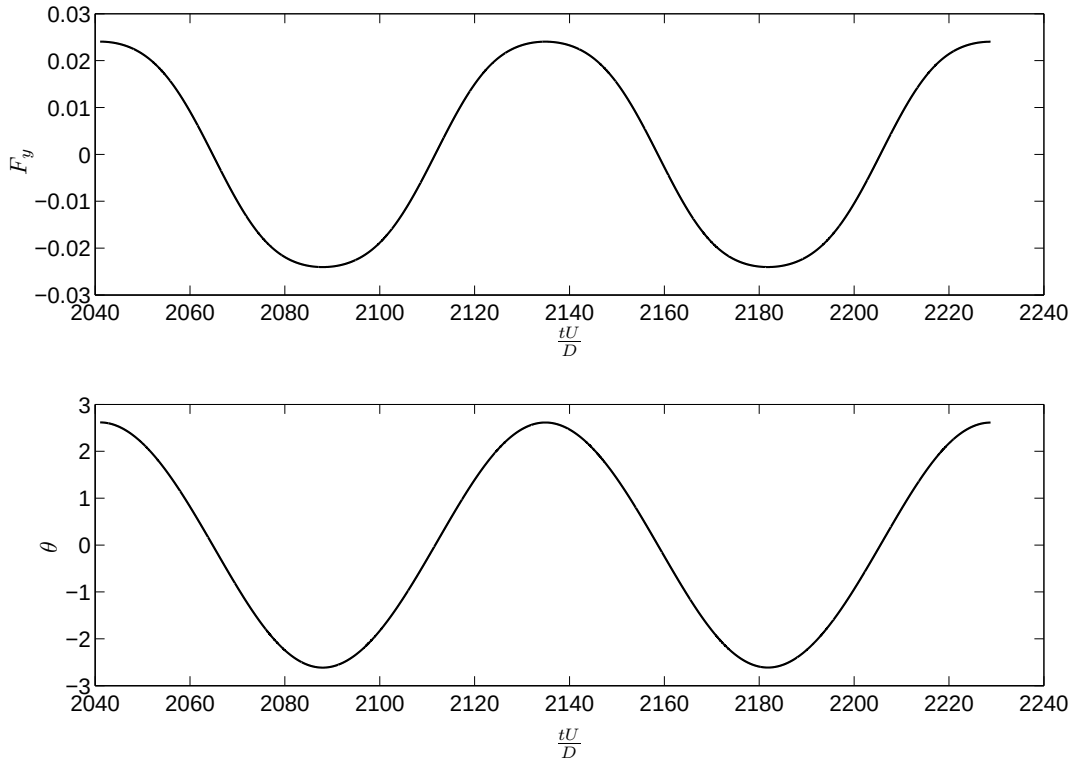

Figure 15: Time history of θ and F_y at $U^* = 90$, $m^* = 40$ and $\zeta = 0.1$

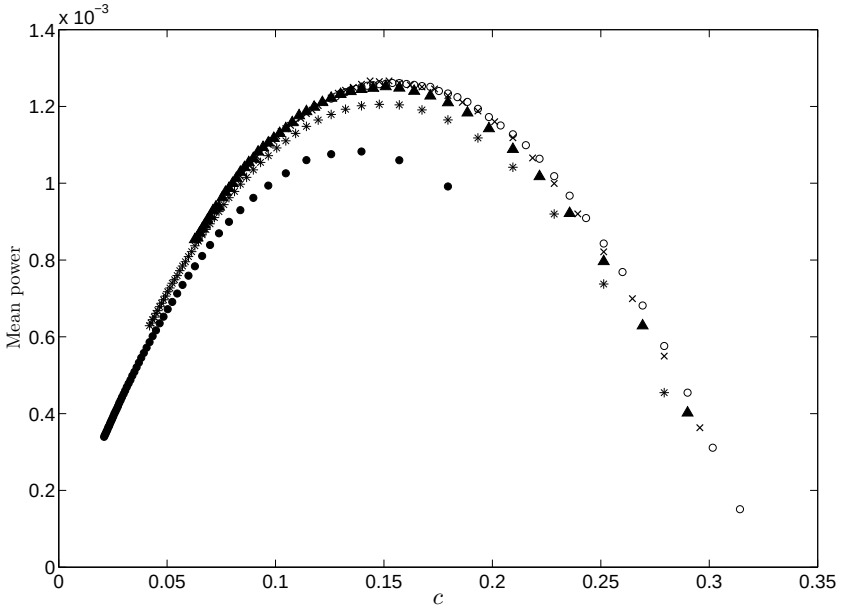

Figure 16: Mean power vs. damping ratio at different m^* $\zeta = 0.1$ (,● $m^* = 10$,✳ $m^* = 20$, ▲ $m^* = 30$, $\times$ $m^* = 40$ and ◯ $m^* = 60$, at Re = 165)

3.4. Comparsion with FSI simulations

Similar trends are captured for both displacement and velocity amplitudes between QSS and FSI simulations (Fig. 17 and 18). Quantitatively a large discrepancy could be observed between QSS and FSI data. Therefore the power also becomes significantly low. The reasoning behind this the fact is that galloping is weak at Re 165 and therefore fluid damping has a significant effect. It was reported by Barrero-Gil et al. (2009) that galloping occur ar Re $\geq$ 159

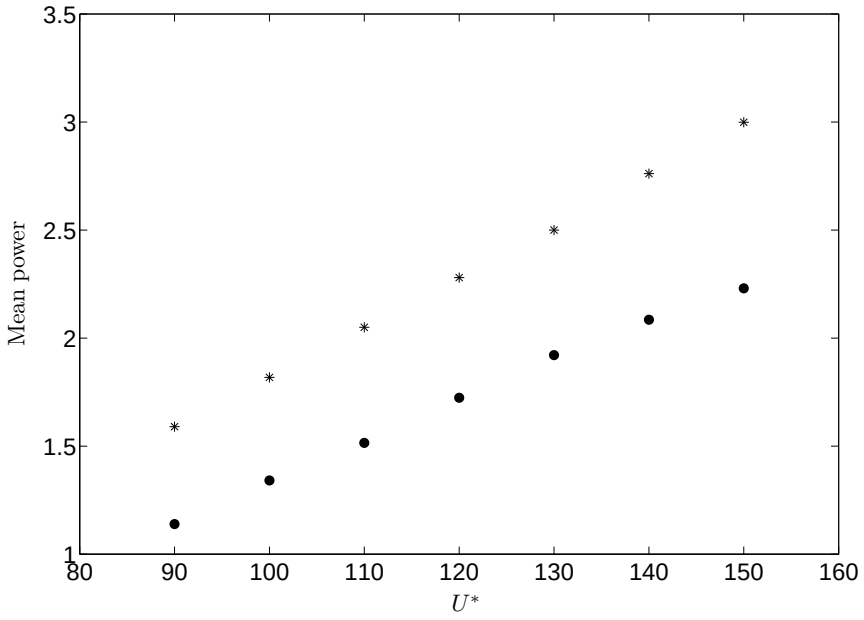

Figure 17: QSS ✳ and FSI ● displacement amplitude data at Re 165 $\zeta = 0.075$ $m^* = 20$

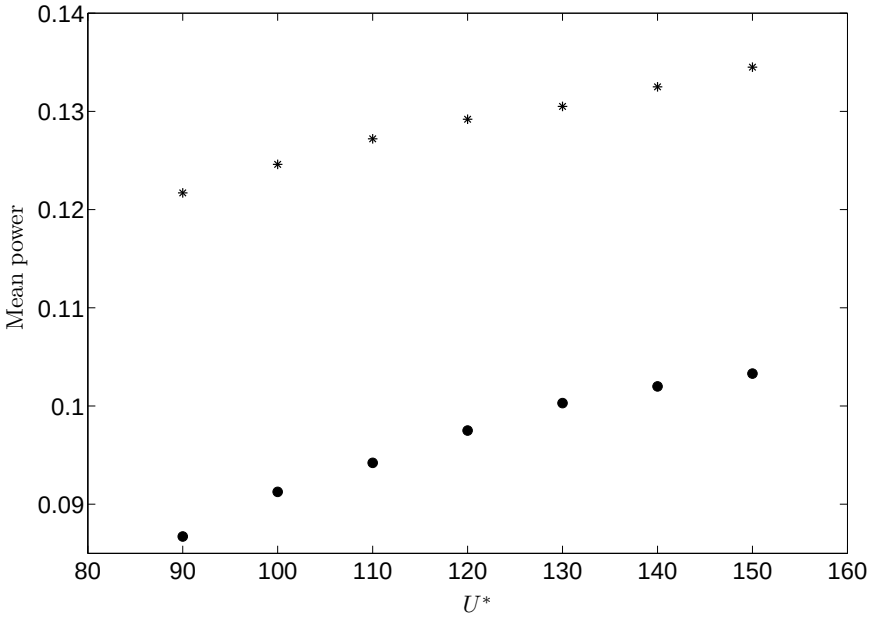

Figure 18: QSS ✳ and FSI ● velocity amplitude data at Re 165 $\zeta = 0.075$ $m^* = 20$

References

Barrero-Gil, A., Alonso, G., Sanz-Andres, A., Jul. 2010. Energy harvesting from transverse galloping. Journal of Sound and Vibration 329 (14), 2873–2883.

Barrero-Gil, a., Sanz-Andrés, A., Roura, M., Oct. 2009. Transverse galloping at low Reynolds numbers. Journal of Fluids and Structures 25 (7), 1236–1242.

Bernitsas, M. M., Raghavan, K., Ben-Simon, Y., Garcia, E. M. H., 2008. VIVACE (Vortex Induced Vibration Aquatic Clean Energy): A new concept in generation of clean and renewable energy from fluid flow. Journal of Offshore Mechanics and Arctic Engineering 130 (4), 041101–15.

Den Hartog, J. P., 1956. Mechanical Vibrations. Dover Books on Engineering. Dover Publications.

Glauert, H., 1919. The rotation of an aerofoil about a fixed axis. Tech. rep., Advisory Committee on Aeronautics R and M 595. HMSO, London.

Joly, A., Etienne, S., Pelletier, D., Jan. 2012. Galloping of square cylinders in cross-flow at low Reynolds numbers. Journal of Fluids and Structures 28, 232–243.

Lee, J., Bernitsas, M., Nov. 2011. High-damping, high-Reynolds VIV tests for energy harnessing using the VIVACE converter. Ocean Engineering 38 (16), 1697–1712.

Leontini, J. S., Lo Jacono, D., Thompson, M. C., Nov. 2011. A numerical study of an inline oscillating cylinder in a free stream. Journal of Fluid Mechanics 688, 551–568.

Leontini, J. S., Th, M. C., Hourigan, K., Apr. 2007. Three-dimensional transition in the wake of a transversely oscillating cylinder. Journal of Fluid Mechanics 577, 79.

Ng, Y., Luo, S., Chew, Y., Jan. 2005. On using high-order polynomial curve fits in the quasi-steady theory for square-cylinder galloping. Journal of Fluids and Structures 20 (1), 141–146.
URL `http://linkinghub.elsevier.com/retrieve/pii/S0889974604001215`

Païdoussis, M., Price, S., de Langre, E., 2010. Fluid-Structure Interactions : Cross-Flow-Induced Instabilities. Cambridge University Press.

Parkinson, G. V., Smith, J. D., 1964. The square prism as an aeroelastic non-linear oscillator. The Quarterly Journal of Mechanics and Applied Mathematics 17 (2), 225–239.

Raghavan, K., Bernitsas, M., Apr. 2011. Experimental investigation of Reynolds number effect on vortex induced vibration of rigid circular cylinder on elastic supports. Ocean Engineering 38 (5-6), 719–731.

Raghavan, K., Bernitsas, M. M., Maroulis, D. E., 2009. Effect of Bottom Boundary on VIV for Energy Harnessing at $8 \times 10^3 < Re < 1.5 \times 10^5$. Journal of Offshore Mechanics and Arctic Engineering 131 (3), 031102.

Sheard, G. J., Fitxgerald, M. J., Ryan, K., Jun. 2009. Cylinders with square cross-section: wake instabilities with incidence angle variation. Journal of Fluid Mechanics 630, 43.

Thompson, M., Hourigan, K., Sheridan, J., Feb. 1996. Three-dimensional instabilities in the wake of a circular cylinder. Experimental Thermal and Fluid Science 12 (2), 190–196. URL http://linkinghub.elsevier.com/retrieve/pii/0894177795000984

Thompson, M. C., Hourigan, K., Cheung, A., Leweke, T., Nov. 2006. Hydrodynamics of a particle impact on a wall. Applied Mathematical Modelling 30 (11), 1356–1369. URL http://linkinghub.elsevier.com/retrieve/pii/S0307904X06000321

Tong, X., Luo, S., Khoo, B., Oct. 2008. Transition phenomena in the wake of an inclined square cylinder. Journal of Fluids and Structures 24 (7), 994–1005. URL http://linkinghub.elsevier.com/retrieve/pii/S088997460800025X